

LUT TENSOR CORE: Lookup Table Enables Efficient Low-Bit LLM Inference Acceleration

Zhiwen Mo^{1,5*}, Lei Wang^{2,5*}, Jianyu Wei^{3,5*}, Zhichen Zeng^{4,5*}, Shijie Cao⁵, Lingxiao Ma⁵
Naifeng Jing¹, Ting Cao⁵, Jilong Xue⁵, Fan Yang⁵, Mao Yang⁵
Shanghai Jiao Tong University¹, Peking University², University of Science and Technology of China³
University of Washington⁴, Microsoft Research⁵

Abstract—As large language model (LLM) inference demands ever-greater resources, there is a rapid growing trend of using low-bit weights to shrink memory usage and boost inference efficiency. However, these low-bit LLMs introduce the need for mixed-precision matrix multiplication (mpGEMM), which is a crucial yet under-explored operation that involves multiplying lower-precision weights with higher-precision activations. Unfortunately, current hardware does not natively support mpGEMM, resulting in indirect and inefficient dequantization-based implementations.

To address the mpGEMM requirements in low-bit LLMs, we explored the lookup table (LUT)-based approach for mpGEMM. However, a conventional LUT implementation falls short of its potential. To fully harness the power of LUT-based mpGEMM, we introduce LUT TENSOR CORE, a software-hardware co-design optimized for low-bit LLM inference. Specifically, we introduce software-based operator fusion and table symmetrization techniques to optimize table precompute and table storage, respectively. Then, LUT TENSOR CORE proposes the hardware design featuring an elongated tiling shape design to enhance table reuse and a bit-serial design to support various precision combinations in mpGEMM. Moreover, we design an end-to-end compilation stack with new instructions for LUT-based mpGEMM, enabling efficient LLM compilation and optimizations. The evaluation on low-bit LLMs (e.g., BitNet, LLAMA) shows that LUT TENSOR CORE achieves more than a magnitude of improvements on both compute density and energy efficiency.

I. INTRODUCTION

The advent of Large Language Models (LLMs) offers disruptive opportunities in various AI applications [4], [6]. However, the deployment of LLMs requires substantial hardware resources. Recent studies suggest larger LLMs often exhibit better model accuracy [27], [57]. This incurs even higher deployment costs, thus posing a formidable barrier to the widespread adoption of LLM [20], [46], [47].

To reduce inference costs, low-bit LLMs have emerged as promising approaches [10], [15], [29], [36]. Among different solutions, weight quantization, i.e., quantizing LLMs with low-precision weights and high-precision activations, has become particularly attractive as it saves memory and computation costs while maintaining model accuracy [14], [35], [66], [72].

Weight quantization shifts the key computation pattern of LLM inference from conventional General Matrix Multiplication (GEMM) to **mixed-precision GEMM (mpGEMM)**, where the weight matrix is in lower precision (e.g., INT4/2/1) and the activation matrix remains in higher precision (e.g.,

FP16/8, INT8). Currently, off-the-shelf hardware does not support mixed-precision operations *natively*. Consequently, most low-bit LLM inference systems have to utilize dequantization-based approaches for mpGEMM [1], [3], [35], [61]. Dequantization upscales low-bit representations to match the hardware-supported GEMM. Such extra operations can become a performance bottleneck in large batch scenarios and miss the opportunity of exploring the full advantages of low-bit LLMs.

Lookup table (LUT) is another popular approach for low-bit computation and well suited for mpGEMM [25], [40], [45]. It replaces sophisticated computation by simple table lookup, thus requiring no dequantization. Despite its advantage, LUT-based mpGEMM GPU kernels often perform worse than dequantization-based kernels due to the inefficient LUT support in hardware, as illustrated in Figure 4. Moreover, a naïve hardware implementation for LUT, although straightforward, does not deliver the promised gain due to the fundamental challenges on extra table overheads, suboptimal hardware design choices, and non-negligible software stack integration efforts (Details in §II-C).

LUT TENSOR CORE addresses these challenges through a *holistic* software and hardware co-design, accelerating low-bit LLM inference with a LUT-based mpGEMM solution. Specifically, LUT TENSOR CORE is unique in the following designs.

Software optimization. To reduce the time to precompute a lookup table, LUT TENSOR CORE aggressively fuses table precomputation with the previous operator, leveraging the fact that table precomputation can always be decomposed into simple element-wise operations. Such fusions result in near zero overhead. To reduce storage overhead, LUT TENSOR CORE exposes and exploits the inherent symmetry of a lookup table for mpGEMM by reinterpreting $\{0, 1\}$ as $\{-1, 1\}$, effectively cutting the table size in half. LUT TENSOR CORE also reduces the table width and supports various activation bit widths by appropriate table quantization, thus further improving efficiency.

Hardware customization. LUT TENSOR CORE customizes the LUT-based Tensor Core design. The software optimizations simplify the implementation of each LUT hardware unit, enabling a reduction in the required registers and multiplexers. Meanwhile, LUT TENSOR CORE incorporates a concise and flexible bit-serial-like circuit to accommodate various combinations of mixed precision operations. This cir-

*Work is done during the internship at Microsoft Research.

cuit enables temporal unfolding, unifying support for various weight bit widths and ensuring the hardware can handle diverse mpGEMM scenarios without excessive chip area. Unlike the conventional tensor core where a square-like tiling shape is preferred, LUT TENSOR CORE favors an elongated tiling shape for LUT-based mpGEMM. This elongated shape improves table reuse and aligns with the typical memory hierarchy in an accelerator, enhancing overall efficiency.

New instruction and compilation support. LUT TENSOR CORE extends the traditional MMA instruction set to LMMA, an LUT-based MMA instruction set with necessary metadata designating the type and shape of the operands. This extension allows seamless integration of LUT-based operations into existing workflows. LUT TENSOR CORE adopts state-of-the-art tile-based deep learning compilers [7], [54], [75]. It leverages the shape information provided in LMMA to recompile LLM workloads. This low-overhead recompilation ensures an efficient and smooth integration of the proposed LUT Tensor Core into existing LLM ecosystem.

Our LUT Tensor Core exhibits a $4\times 6\times$ reduction in power and area compared to the conventional Tensor Core. To validate the performance enhancement of mpGEMM, we integrate the design and instructions for LUT TENSOR CORE into Accel-Sim [28], a GPU hardware simulator. The results show that LUT TENSOR CORE uses only 16% of the area of a conventional Tensor Core while achieving even higher mpGEMM performance.

In order to evaluate the end-to-end model inference speedup, we construct a tile-level cost model for LUT TENSOR CORE-equipped GPU. Results show that under nearly identical LLM accuracy, an accelerator equipped with LUT TENSOR CORE can achieve up to $6.93\times$ inference speedup while only requiring 38.3% of the original Tensor Core’s area, i.e., $20.9\times$ compute density and $11.2\times$ energy efficiency improvements.

Our contributions can be summarized as follows:

- We propose LUT TENSOR CORE, a software-hardware co-design for LUT-based mpGEMM to boost the inference efficiency of low-bit LLMs.
- Experiments show the proposed LUT TENSOR CORE achieves remarkable Power, Performance, and Area (PPA) gains. It exhibits substantial inference speedups for BitNet and quantized representative LLMs like LLAMA, OPT, and BLOOM, validating the efficacy of our approach.
- Beyond efficiency, our design can accommodate a wide range of weight (e.g., INT4/2/1) and activation precisions (e.g., FP16/8, INT8). Moreover, LUT TENSOR CORE can smoothly integrates with existing inference hardware and software stacks with our extended LMMA instructions and compilation optimizations.

II. BACKGROUND AND MOTIVATION

A. Low-Bit LLM Inference

Nowadays, LLMs mainly rely on the decoder-only transformer architecture shown as Fig. 1 to generate contextually cohesive output [58]. Specifically, LLMs are built with

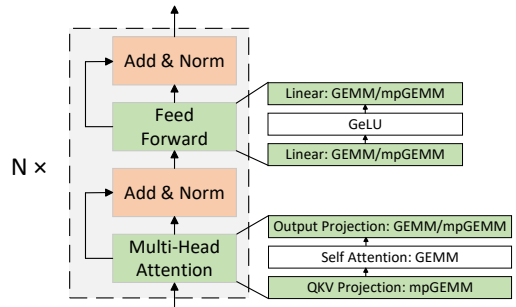


Fig. 1: Decoder-only transformer blocks in LLMs. The primary computations are GEMM operations (or mpGEMM operations with weight quantization).

sequential transformer layers, where each transformer layer contains a multi-head attention block followed by a feed forward block. In both multi-head attention and feed forward block, the primary computations are GEMM operations or mpGEMM operations with weight quantization. The studies on scaling law [20], [27] suggest that LLMs will produce better results when scaling up transformer layers. Consequently, there is a rapid growth in the scale of models, which in turn requires significant hardware resources. For example, LLAMA-2-70B [57] consumes 140GB of memory for its model weights alone (in FP16), far exceeding the capacity of a modern GPU like NVIDIA A100 or H100. This imposes a considerable challenge for LLM deployment.

To reduce inference costs in LLM deployment, low-bit quantization has become a popular approach [10], [12]. It reduces the precision of numerical representations of a model, thus decreasing memory footprint and computation time. Nowadays, it becomes a common practice to release LLMs with its low-bit versions [56], [67].

Quantization is known to degrade model accuracy. Among different choices, *weight quantization* is preferred over activation quantizations [33], [35]. This is because the values of model weights are known ahead of time and thus can be quantized offline. Weights can be quantized to 4-bit, 2-bit, and even 1-bit without impacting model accuracy significantly [14], [39], [56], [60], [67]. Conversely, activations are generated on-the-fly with a high variance, noticeably presented as dynamic outliers [10], [17], [64]. These outliers can lead to significant accuracy degradation. In some case, it is difficult to maintain model accuracy even with 8-bit activations.

Although the trend is clear, finding the right bit-width for weight and activation is complex, as it needs to strike a delicate balance between model size, computational speed, and model accuracy per user demands. Different combinations of weight and activation bit-widths have been explored in different models and scenarios [10], [14], [15], [18], [60], suggesting that no universal solution that fits all scenarios.

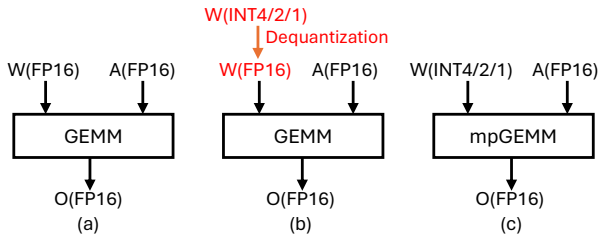


Fig. 2: (a) GEMM, (b) Indirect mpGEMM: mpGEMM to GEMM by dequantization, (c) Direct mpGEMM.

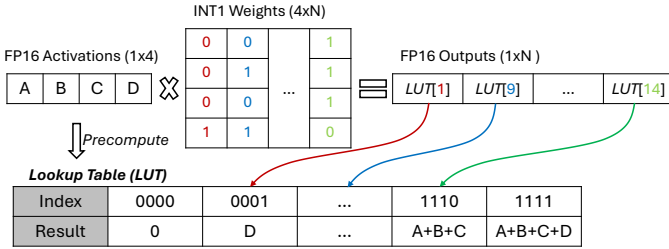


Fig. 3: A naive LUT-based mpGEMM example of FP16 activations and INT1 weights. With the precomputed table, a table lookup can replace a dot product of 4-element vectors.

B. mpGEMM in Low-Bit LLM Inference

The use of various bit-width for weights and activations leads to a unique requirement of mixed-precision General Matrix Multiplication (mpGEMM), where the weight matrix is in lower precision and the activation matrix remains in higher precision. Figure 2 shows an example of INT4/2/1 multiplied by FP16. Currently, commercial LLM inference hardware, such as GPU and TPU, does not support mpGEMM natively. They only focus on conventional GEMM where two inputs are with the same format and bit-width.

Dequantization-based mpGEMM upscales low-precision weights to match the high-precision activations so that conventional GEMM is applicable [2], [61]. Although it can accommodate various combinations of precisions, dequantization requires extra operations and can become a performance bottleneck. Meanwhile, as the GEMM is still computed in high precision, dequantization-based mpGEMM cannot take the full advantage of low-precision computation.

LUT-based mpGEMM is an alternative approach that uses lookup tables (LUTs) to implement mpGEMM [25], [40], [45]. It precomputes dot products of high-precision activations with a limited set of low-precision weights and replaces the computation by simple lookups in the resulting table. LUT-based mpGEMM can eliminate most multiplications and reduce additions, thus presumably improving efficiency. Figure 3 illustrates a naive example of using LUT for FP16 activations multiplied by INT1 weights. In this case, the activation vector length is 4, resulting in a lookup table of size 16. This allows a table lookup to replace a dot product of 4-element vectors. For longer activations or higher-bit weights, a larger lookup table is required.

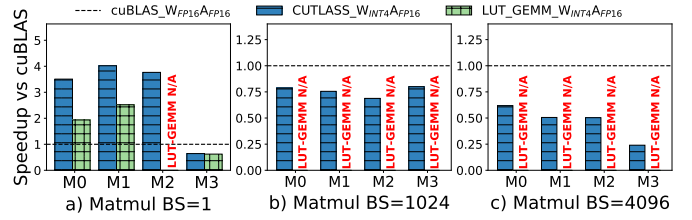


Fig. 4: Dequantization-based mpGEMM kernels (CUTLASS) vs. LUT-based mpGEMM kernels (LUT_GEMM) on A100 GPU. $W_{INT4}A_{FP16}$ means weights in INT4 and activations in FP16, and so on so forth. The $W_{FP16}A_{FP16}$ cuBLAS version serves as a baseline. Matrix shapes M0-M3 are extracted from the linear layers of the LLAMA2-70B model across batch sizes (BS) 1, 1024, and 4096.

Despite its theoretical advantage, LUT-based mpGEMM kernels are often less effective than dequantization-based kernels on existing LLM inference hardware like GPUs, due to the limited LUT support. Figure 4 compares the performance of the LUT-based mpGEMM kernel in [45] to the dequantization-based mpGEMM kernel in CUTLASS [2] on A100 GPU. The results show that the dequantization-based kernel always outperforms the LUT-based kernel. When batch size is large, the LUT-based kernel performs several orders of magnitude worse because of the table access overhead. Thus we denote its performance as N/A in the figure. Moreover, the dequantization-based mpGEMM kernel performs worse than the $FP16 \times FP16$ GEMM cuBLAS kernel when batch size is large, due to the overhead of the additional dequantization operation. This motivates us to customize a LUT-base design for mpGEMM.

C. Challenges of LUT-based mpGEMM Hardware

At first glance, LUT-based hardware offers great simplicity, as it only requires register or memory for table storage and multiplexers for table lookup. However, our study suggests that a naive LUT hardware design cannot deliver the promised gains. Numerous challenges and unexplored design aspects significantly affect system performance. This includes:

Table precompute and storage. LUT-based approach requires precomputing the table, which can introduce area and latency overhead. The table can also occupy more storage space. This could diminish the efficiency gains.

Bit-width flexibility. As discussed in §II-A, LUT-based mpGEMM needs to support different bit-width combinations, e.g., $INT4/2/1 \times FP16/FP8/INT8$, while handling each case separately may consume excessive chip area. Achieving efficiency and flexibility at the same time poses a new challenge.

LUT tiling shape. The tiling of the LUT unit can significantly impact performance, as a suboptimal tiling shape increases storage costs and reduces opportunities for table reuse.

Instruction and compilation. LUT-based mpGEMM requires a new instruction set. The conventional compilation stack optimized for standard GEMM hardware may not provide optimal mapping and scheduling plans for the mpGEMM

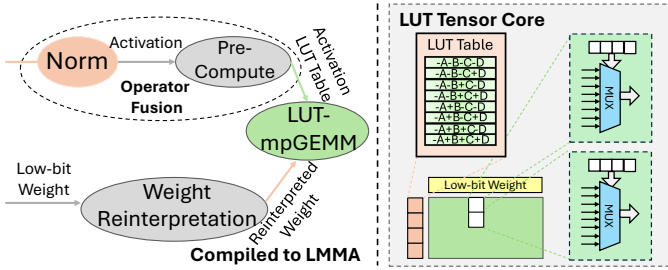


Fig. 5: Workflow of LUT TENSOR CORE-accelerated low-bit LLMs.

instruction set with a different tiling shape. This increases the efforts to integrate the LLM inference software stack with the new LUT design.

III. LUT TENSOR CORE DESIGN

To unleash the full potential of LUT-based mpGEMM, we introduce LUT TENSOR CORE, a software-hardware co-design approach aimed at addressing the aforementioned efficiency, flexibility, and compatibility challenges (§II-C). Fig. 5 illustrates the overview of LUT TENSOR CORE. Different from the conventional hardware-based solution for LUT table precompute and storage that may introduce significant hardware overheads, LUT TENSOR CORE designs software-based optimizations (§III-A) to optimize the LUT table precompute and storage: precomputing the LUT table for the input activation tensor is performed by operator fusion, while the input weight tensor is reinterpreted to enable table storage optimizations. On the hardware side, LUT TENSOR CORE features a simplified microarchitecture (§III-B), that enhances efficiency for mpGEMM processing and supports flexibility for various bit-width data types. To integrate LUT TENSOR CORE into existing deep learning ecosystem, we design the LUT-based Matrix Multiply-Accumulate (LMMA) instruction set to expose the LUT TENSOR CORE for programming mpGEMMs and implements the compilation stack to schedule the end-to-end LLM execution (§III-C).

A. Software-based Table Optimization

As introduced in §II, LUT-based mpGEMM needs additional table precomputing process and storage to store the precomputed results. Naively, the precomputed dot products of a length K activation vector on the W_BIT weight require $(2^{W_BIT})^K$ entries for the table. For each activation element, multiplying it with the W_BIT weight has 2^{W_BIT} possible results, constructing the precompute table for this activation element. Therefore, the precomputed table has $(2^{W_BIT})^K$ entries for a length K activation vector. Fig. 3 shows the lookup table with 2^4 entries for $K = 4, W_BIT = 1$.

A commonly-used optimization is bit-serial [26] that represents a W_BIT integer as W 1-bit integers and performs multiplication over 1-bit integers with bit shift. This paradigm can reuse the precompute table on 1-bit, and therefore reduces the table size to 2^K . However, this table size still has significant hardware overheads.

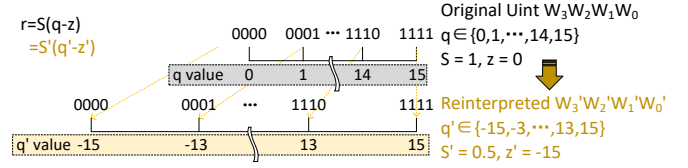


Fig. 6: Reinterpreting 0,1 to -1,1 to enable symmetry, thereby cutting the table size by half.

To address these overheads, LUT TENSOR CORE proposes operator fusion to reduce the table precompute time, weight reinterpretation and table quantization to reduce the table size.

1) Precomputing lookup table with operator fusion:

The LUT-based mpGEMM requires precomputing the dot production of high-precision activation and a set of low-precision weights as a table for the later lookup operations. A conventional hardware implementation is positioning the precompute unit adjacent to the LUT unit and performing the table precompute for each LUT unit on-the-fly. However, this implementation may significantly introduce hardware cost.

Fortunately, the table precompute described above is an element-wise operation where each element is the production of an activation value and a combination $\{0, 1\}$ of K that can be processed by a general-purpose compute unit (e.g., CUDA Cores in GPU). Moreover, the precompute table can also be shared by LUT units instead of precomputing a table for each LUT unit to reduce the redundant precomputation. Therefore, we can enable a one-time precompute kernel for the input activation tensor and write back the precompute table to memory. Then the LUT units can load the precompute table to the register and perform table lookups. Furthermore, as introduced in Fig. 1, the preceding operator of a mpGEMM is normalization that is also an element-wise operator. The table precompute operation can be fused into the preceding operators for further optimizations, which will be detailed in §III-C2. This helps to mitigate the table precompute overhead to almost zero as evaluated in §IV-E1.

2) Reinterpreting weight for table symmetrization:

The 2^K table length of precomputing a length K activation vector introduces cost in both table storage and table accesses. Fortunately, we observed the symmetrization property of integers that the integer representation can be symmetric around zero with a math-equivalent linear transformation.

Assume K weights $[W_{K-1}, \dots, W_2, W_1, W_0]$ are represented as a K -bit integer:

$$r = s(q - z) \quad (1)$$

where r is the real value, s is the scale factor, z is the bias, and q is the integer representation to K bits.

To transform such representation to be symmetric around zero, we map q to make it symmetric to zero and adjust s and z correspondingly:

$$q' = 2q - (2^K - 1), \quad s' = s/2, \quad z' = 2z + 1 - 2^K \quad (2)$$

Fig. 6 shows the example of transforming the 4-bit unsigned integers. By calculating the s' and z' , q' is mapped from $\{0, 1, \dots, 14, 15\}$ to $\{-15, -13, \dots, 13, 15\}$, which is symmetric around zero.

Let's consider a dot product between the binary representation $W_3W_2W_1W_0 = 0100$ and variables A, B, C, D . Initially, the binary values $\{0, 1\}$ are interpreted as $\{0, 1\}$. The calculation proceeds as follows:

$$r = s \cdot (q - z) = 1 \cdot (B - 0) = B$$

After reinterpretation, the binary values $\{0, 1\}$ are redefined to mean $\{-1, 1\}$, with the scale factor s' adjusted to 0.5 and the bias z' recalculated as $-(A + B + C + D)$. The updated computation is:

$$r = s' \cdot (q' - z') = 0.5 \cdot ((-A + B - C - D) + (A + B + C + D)) = B$$

It's clear that the two expressions remain mathematically equivalent.

As the table entries are symmetric about zero, the lookup table exhibits properties similar to odd functions. Assuming the index is a 4-bit value $W_3W_2W_1W_0$, a naive implementation of the lookup table (LUT) requires $2^4 = 16$ entries. However, it can be observed that the following property, akin to that of odd functions, holds:

$$\text{LUT}[W_3W_2W_1W_0] = -\text{LUT}[\sim(W_3W_2W_1W_0)] \quad (3)$$

Therefore, the number of entries in the LUT can be reduced to half of the original, which is $2^{4-1} = 8$, and the equation becomes:

$$\text{LUT}[W_3W_2W_1W_0] = \begin{cases} -\text{LUT}[\sim(W_2W_1W_0)], & \text{if } W_3 = 1 \\ \text{LUT}[W_2W_1W_0], & \text{if } W_3 = 0 \end{cases} \quad (4)$$

Therefore, given a length K activation vector, table symmetrization can reduce the table length to 2^{K-1} . The table size not only affects the computational operations required during the precompute stage, but also the multiplexers (MUX) size. Furthermore, each entry in the table also needs to be broadcast to N PEs, typically 64 or 128, for dot product computations. Such an optimization significantly reduces the broadcasting overhead and the MUX selection overhead, thereby enhancing the energy efficiency and area efficiency of the circuit.

Note that $W_3W_2W_1W_0$ in Equation 4 are all weights, which will not be modified in inference. So, the bit-level negation can be done by offline weight transformation and the equation can further be simplified to:

$$\text{LUT}[W'_3W'_2W'_1W'_0] = \begin{cases} -\text{LUT}[W'_2W'_1W'_0], & \text{if } W'_3 = 1 \\ \text{LUT}[W'_2W'_1W'_0], & \text{if } W'_3 = 0 \end{cases} \quad (5)$$

This simplification can eliminate the negation operation in circuit design, which will be introduced in §III-B.

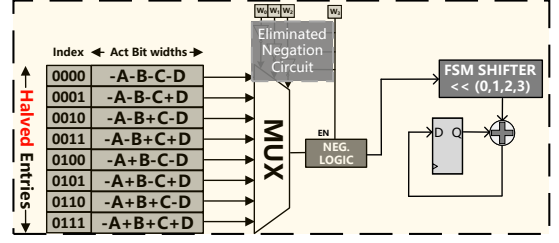


Fig. 7: Optimized LUT unit with bit-serial.

3) **Table Quantization:** Table symmetrization can reduce the table size by half. Moreover, for high precision activations, such as FP32 or FP16, we utilize table quantization techniques to quantize the precomputed table elements to a lower, unified precision, such as INT8. This approach offers flexibility by supporting multiple activation precisions and efficiency by reducing storage requirements through lower precision table elements.

Although table quantization might potentially affect model accuracy, it provides a significant advantage over conventional activation quantization. Traditional activation quantization cannot leverage dynamic, fine-grained quantization due to efficiency concerns. In contrast, table quantization allows for dynamic, fine-grained quantization during the precomputation phase. For instance, with a group size of 4 activation elements, we perform quantization for each generated table with 8 precomputed dot-products. This method is expected to maintain higher accuracy compared to conventional activation quantization. Our empirical experiments, as discussed in § IV-E2, confirm this expectation. The results demonstrate that the impact on accuracy when using INT8 quantization for the table elements is minimal, thereby validating the effectiveness of our approach.

B. LUT TENSOR CORE Microarchitecture

1) **Simplified LUT unit design with bit-serial:** By leveraging software-based precompute fusion and weight reinterpretation, the hardware cost for customizing each individual LUT unit is significantly reduced. Each LUT unit is simple and easy to scale out. Fig. 7 illustrates our LUT unit design. In comparison to a naive design, the registers needed to store the LUT can be halved, and the cost of the table broadcasting and MUX is also halved. Moreover, as depicted in equation 5, portion of the bit-level negation circuit can be eliminated from each LUT unit, resulting in lower area and power consumption in the hardware. To support flexible bit-widths for weights, we employ a bit-serial circuit architecture [26], [65]. This design unfolds the weight bit-width to W_BIT cycles, thereby enabling the processing of different bit-widths in a serialized manner. This bit-serial approach allows the hardware to adapt to various precision levels without the need for multiple distinct hardware implementations.

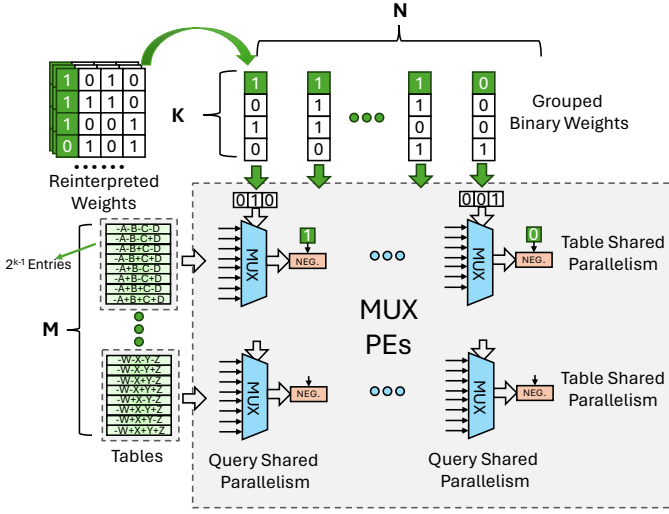


Fig. 8: Elongated MNK tiling of LUT TENSOR CORE. LUT TENSOR CORE requires a larger N (e.g., 64/128) to maximize table reuse, along with a suitably sized K (e.g., 4) for a cost-efficient table size.

2) **Elongated LUT tiling:** The selection of dimensions M , N , and K is crucial for the performance of LUT TENSOR CORE, with traditional choices for MAC-based Tensor Cores potentially leading to suboptimal performance in this context. As illustrated in Fig. 8, a MNK Tile’s LUT Array comprises M tables, N sets of weights, and $M * N$ MUX-based units. Each table contains $M \times 2^{K-1}$ entries, with each entry needing to be broadcast to N MUX units; each set of Grouped Binary Weights includes K bits, which must be broadcast to M MUX units to act as select signals for the MUX. The total table size is given by the equation:

$$\text{Total Table Size} = M \times 2^{K-1} \times \text{LUT_BIT} \quad (6)$$

and the size for grouped binary weights is given by:

$$\text{Grouped Binary Weights Size} = K \times N \times \text{W_BIT} \quad (7)$$

where LUT_BIT is the bit width of the LUT entries, and W_BIT is the bit width of the weights.

LUT TENSOR CORE prefers elongated tiling shape. With large K , the size of table entries explodes exponentially, whereas N represents the potential reuse of each table entry across multiple MUX units. Intuitively, we need to find a balance with a suitably sized K , a larger N , and a smaller M —a configuration that diverges from the typical demands of conventional GPU Tensor Cores. Furthermore, we must consider the impact of this shape on tiling, as a more square-like tiling configuration can lead to lower I/O traffic. Therefore, we also strive to balance the size of the LUT and weight within a tile as closely as possible. In §IV-B2, we conduct extensive and comprehensive experiments to explore the design space for MNK tiling, verifying elongated tiling shapes achieve better efficiency.

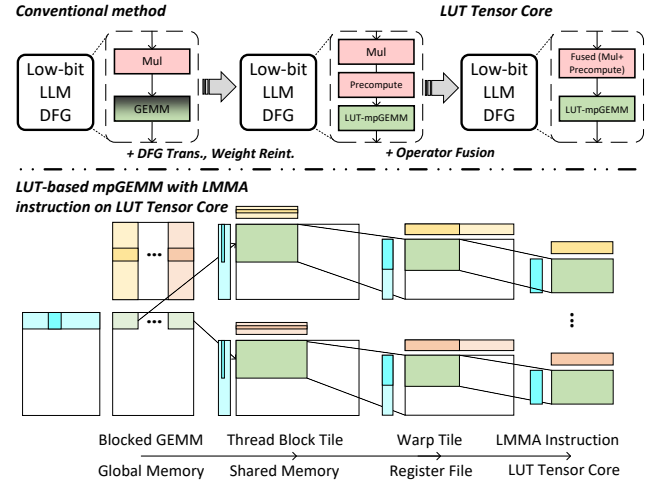


Fig. 9: Compilation for LUT-based mpGEMM. Elongated tile for enhancing data reuse in mpGEMM.

C. Instruction and Compilation

To effectively integrate LUT TENSOR CORE into the existing GPU architecture and ecosystem, we propose a new set of instructions and have developed a compilation stack based on state-of-the-art DNN compilers [7], [54], [75]. Our compilation stack has been enhanced with specialized intrinsics and optimizations, specifically designed to leverage the unique capabilities of LUT TENSOR CORE.

1) **LUT-based MMA instructions:** To enable programming with LUT TENSOR CORE, we define a set of LMMA (LUT-based MMA) instructions as an extension of the MMA instruction set in GPU.

$$\text{lmma}\{M\}\{N\}\{K\}\{A_{dtype}\}\{W_{dtype}\}\{Accum_{dtype}\}\{O_{dtype}\}$$

The above formula shows the format of LMMA instructions, which is similar to MMA. Specifically, the M , N , and K indicates the shape of the LUT TENSOR CORE. A_{dtype} , W_{dtype} , $Accum_{dtype}$ and O_{dtype} indicate the data type of the inputs, accumulation and the output, respectively. Similar to MMA instructions, each LMMA instruction is scheduled to a warp of threads for execution. This warp of threads will calculate the formula $O_{dtype}[M, N] = A_{dtype}[M, K] \times W_{dtype}[N, K] + Accum_{dtype}[M, N]$. The LMMA instructions are similar to MMA instructions, while have different shapes and data types.

2) **Compilation support and optimizations:** We implemented the LUT-based mpGEMM kernel generation and end-to-end LLM compilation with LUT TENSOR CORE on top of TVM [7], Roller [75] and Welder [54]. Specifically, the compilation stack encompasses the following key aspects and Fig. 9 shows an example of compilation on the LLAMA model:

- **DFG Transformation.** Given the model represented in data-flow graph (DFG), we transform the mix-precision GEMM

operator to a precompute operator and the LUT-based mpGEMM operator. This transformation is implemented as a graph optimization pass in Welder.

- **Operator Fusion.** Operator fusion is a widely-used compiler technique to optimize the end-to-end model execution by reducing memory traffic and runtime overhead. We registered the precompute and the LUT-based mpGEMM operator and represented the required tile-based representation in Welder, enabling reusing Welder to do operator fusion. As shown in Fig. 9, the element-wise precompute operator is fused with the element-wise Norm operator prior to the GEMM operator in LLAMA, which further reduces the table precompute overhead.
- **LUT-based mpGEMM Scheduling.** Similar to GEMM, scheduling LUT-based mpGEMM operator requires careful considering tiling on the memory hierarchy for performance. As shown in Figure 9, GPUs have a memory hierarchy of global memory, shared memory, registers, and tiling on the memory hierarchy can significantly improve the data reuse on on-chip memory to improve performance. Conventional tiling strategies [7], [73], [75] for GEMM assume the same data type on both activation and weight and focus on adjusting the tiling shape on memory hierarchy. However, mpGEMM has different data types on activation and weight, resulting in different memory behaviors for tensors of different data types. We observed the influence of different data types on memory hierarchy is the actual memory transactions. Therefore, we represent the tiling with the actual memory size instead of tiling shape, and register the shape of LMMA instructions and this tiling calculation in Roller’s rTile interfaces to schedule the proper tiling configurations.
- **Code Generation.** With the finalized scheduling plans, code generation is performed using TVM. Specifically, the LMMA instructions are registered as intrinsics in TVM, and TVM can follow the scheduling to generate the kernel code with LMMA instructions.

IV. EVALUATION

In this section, we conduct a comprehensive and systematic evaluation of LUT TENSOR CORE to validate its efficiency in accelerating low-bit LLM inference. Initially, we assess the hardware efficiency gains of LUT TENSOR CORE via detailed PPA benchmarking (§IV-B). Then, kernel-level experiments are conducted to illustrate the acceleration of mpGEMM (§IV-C). Following this, we perform end-to-end inference evaluation on commonly-used LLMs to demonstrate the practical performance improvements (§IV-D). We then delve into the effectiveness of our software optimizations on table precompute fusion and table quantization (§IV-E). Finally, we provide a holistic comparison of model accuracy and efficiency with previous accelerator designs (§IV-F).

A. Experimental Setup and Methodology

1) **Hardware PPA benchmarks:** We compare LUT TENSOR CORE approach with two baselines: Multiply-Accumulate

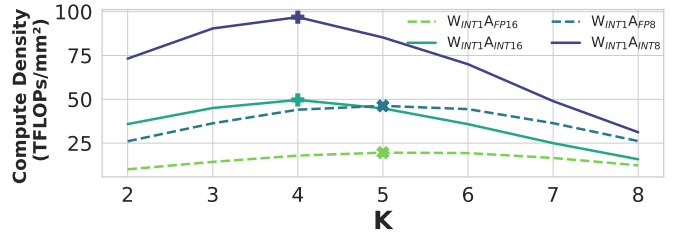


Fig. 10: K-axis design space exploration for LUT TENSOR CORE’s dot product unit. $K = 4$ is the optimal in general.

(MAC)-based Tensor Core and Addition (ADD)-based Tensor Core. MAC represents the typical design in current GPUs which needs dequantization to support mpGEMM. ADD adopts the bit-serial computing proposed in [26] to support mpGEMM, where every bit of weights needs one addition. We implement LUT TENSOR CORE and baselines in Verilog and use Synopsys’s Design Compiler [55] and the TSMC 28nm process library for synthesizing circuits and generating PPA data. We apply DC’s medium effort level targeting 1GHz to ensure a fair comparison across all designs.

2) **Kernel-level evaluation:** Considering that GPUs are the most widely-used hardware for LLM inference today and are equipped with MAC-based Tensor Cores, they provide an ideal platform for comparison and comprehensive evaluation. For mpGEMM kernel-level evaluation, we set the NVIDIA A100 GPU as the baseline. We employ Accel-Sim [28], an open-source state-of-the-art simulator, to run these experiments. Necessary modifications to the configuration and trace files in Accel-Sim allow us to simulate both the original A100 and the LUT TENSOR CORE-equipped A100.

3) **Model end-to-end evaluation and analysis:** To extend our evaluation to real LLMs, we utilize four widely-used open-source LLMs: LLAMA-2 [57], OPT [71], BLOOM [32], and BitNet [60]. As Accel-Sim becomes infeasible for end-to-end LLM experiments due to its extremely slow simulation speed for large trace file size, we develop a tile-based simulator to support end to end inference evaluations, which will be detailed in §IV-D.

B. Hardware PPA Benchmarks

1) **Dot Product unit microbenchmark:** As discussed in § III-B2, the parameter K in LUT tiling is crucial for compute efficiency. In the hardware experiments, we fixed M and N to 1 and varied K (i.e., a dot product unit of K -element vectors) to explore its impact on compute density. Excessively large K could potentially lead to an exponential growth in lookup table entries, thereby increasing area without proportional gains in efficiency. Conversely, smaller K may lead to an inefficient dominance of computations being handled by adders, which could reduce compute density. As shown in Fig. 10, we found INT operations achieve optimal density at $K = 4$, while floating-point operations peak at $K = 5$ but perform similarly well at $K = 4$. Therefore, we adopt $K = 4$ for all subsequent LUT-based designs.

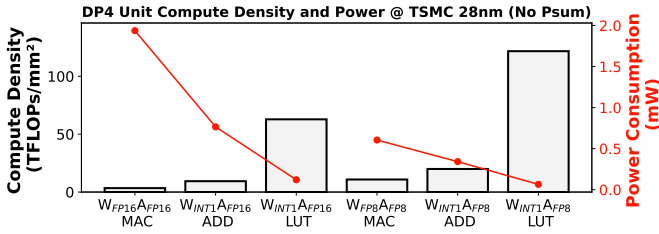


Fig. 11: PPA comparison across MAC-based Tensor Core, ADD-based Tensor Core, and LUT TENSOR CORE’s DP4 implementations. LUT TENSOR CORE’s DP4 unit has significant compute density and power advantages.

Following $K = 4$, we conduct benchmarks on dot product implementations using MAC-based, ADD-based, and LUT TENSOR CORE approach across various data formats. The configurations assessed include conventional symmetric precision with MAC ($W_{FP16}A_{FP16}$, $W_{FP8}A_{FP8}$) and mixed precision ($W_{INT1}A_{FP16}$, $W_{INT1}A_{FP8}$) using both ADD and LUT approaches. As depicted in Fig. 11, the LUT-based approach achieved the highest compute density, reaching 61.55 TFLOPs/mm² with $W_{INT1}A_{FP16}$, substantially surpassing the conventional MAC configuration which registered only 3.39 TFLOPs/mm² with $W_{FP16}A_{FP16}$. The behaviour of power efficiency exhibits similar performance. Specifically, under the A_{FP16} format, the LUT TENSOR CORE approach delivered an 18.13 \times increase in compute density and reduced power consumption by 15.45 \times compared to MAC methods.

Furthermore, we conduct weight-bit scaling experiments on the $W_{INTX} \times A_{FP16}$ DP4 units for MAC-based, ADD-based, and LUT-based(LUT TENSOR CORE) implementations. The experiments are configured with the tensor core’s N dimension set to 4 to match the A100’s configuration. As shown in Fig. 12, the conventional LUT-based implementation does not have area advantages compared to the MAC baseline when the weight is more than 2-bit. The main area efficiency bottleneck is the table precompute and storage overheads. ADD-based implementations also only surpass the MAC baseline in the 1-bit and 2-bit cases. By optimizing the table storage overhead and the precompute overhead with symmetry-based table reduction and compilation optimizations, our LUT TENSOR CORE implementation outperforms all the baselines up to a weight bit-width of 6 and delivers much better area efficiency compared to the conventional LUT implementation.

2) **Tensor Core benchmark:** In previous experiments, we confirm the superiority of the LUT-based design within the basic DP units. In this section, we scale our investigation to the Tensor Core level, incorporating a design space exploration to identify optimal MNK configurations. We align the computational capabilities with those of the A100 INT8 Tensor Core, which delivers 1024 operations per cycle per Tensor Core, setting $M \times N \times K = 512$ for extensive design space exploration. Our data types range from A_{FP16} to A_{INT8} and include various weight bit-widths. We compare our LUT TENSOR CORE approach against MAC- and ADD-

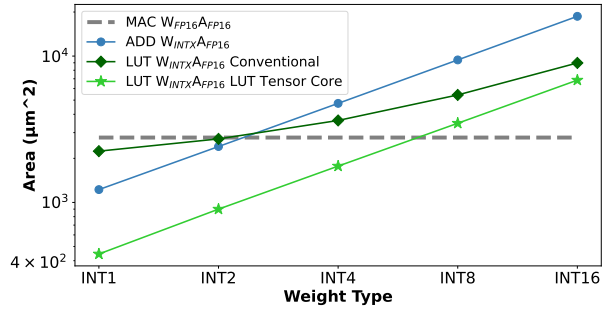


Fig. 12: Area comparison of MAC-based Tensor Core, ADD-based Tensor Core, and LUT TENSOR CORE’s DP4 units across weight bit-widths in $W_{INTX} \times A_{FP16}$. Conventional LUT implementation does not have area advantages.

based approaches. To make a fair comparison across difference activation data types, we don’t enable table quantization for this benchmark.

As shown in Fig. 13, the dashed lines represent the contours where the minimum Area*Power point for each design methodology lies among all data points. Our results demonstrate that across 12 sets of experiments with different activation data formats and weight bit-widths, the LUT TENSOR CORE method achieves the smallest area and lowest power consumption, except in the $W_{INT8}A_{INT4}$ case. Notably, with 1-bit weights, the LUT TENSOR CORE approach exhibits a 4 \times -6 \times reduction in power and area compared to the MAC-based Tensor Core design. After our design space exploration, we identify the optimal MNK configuration for the LUT TENSOR CORE as $M2N64K4$.

C. Kernel-level Evaluation

Building on the PPA superiority of the LUT TENSOR CORE, we employ Accel-Sim, a SOTA GPU simulator, to validate not only the robust computational power of LUT TENSOR CORE in mpGEMM operations but also their compatibility with existing GPU architectures. The mpGEMM benchmarks leverage the configuration used in the LLAMA2-13B model, with $M = 2048$, $N = 27648$, and $K = 5120$. The dataflow of mpGEMM is designed to be cutlass-like and output-stationary, with tiling shapes optimized by Roller [75] for efficient data reuse. For instance, a good candidate for $W_{INT1}A_{INT8}$ tiling sets the Thread Block tile to [128, 512, 32] and the Warp tile to [64, 256, 32].

As illustrated in Fig. 14, each subplot presents results where the leftmost bar represents actual measurements, followed by three simulated results: ideal peak performance, simulated measured performance, and performance after applying several times the baseline’s register capacity. The latter adjustment addresses bottlenecks caused by insufficient register capacity, which limit large tiling and systemically bind performance to memory constraints. This modification ensures that speedups are not mistakenly attributed to improved memory bandwidth.

Experimental results confirm that LUT TENSOR CORE significantly outperforms traditional MAC-based Tensor Core

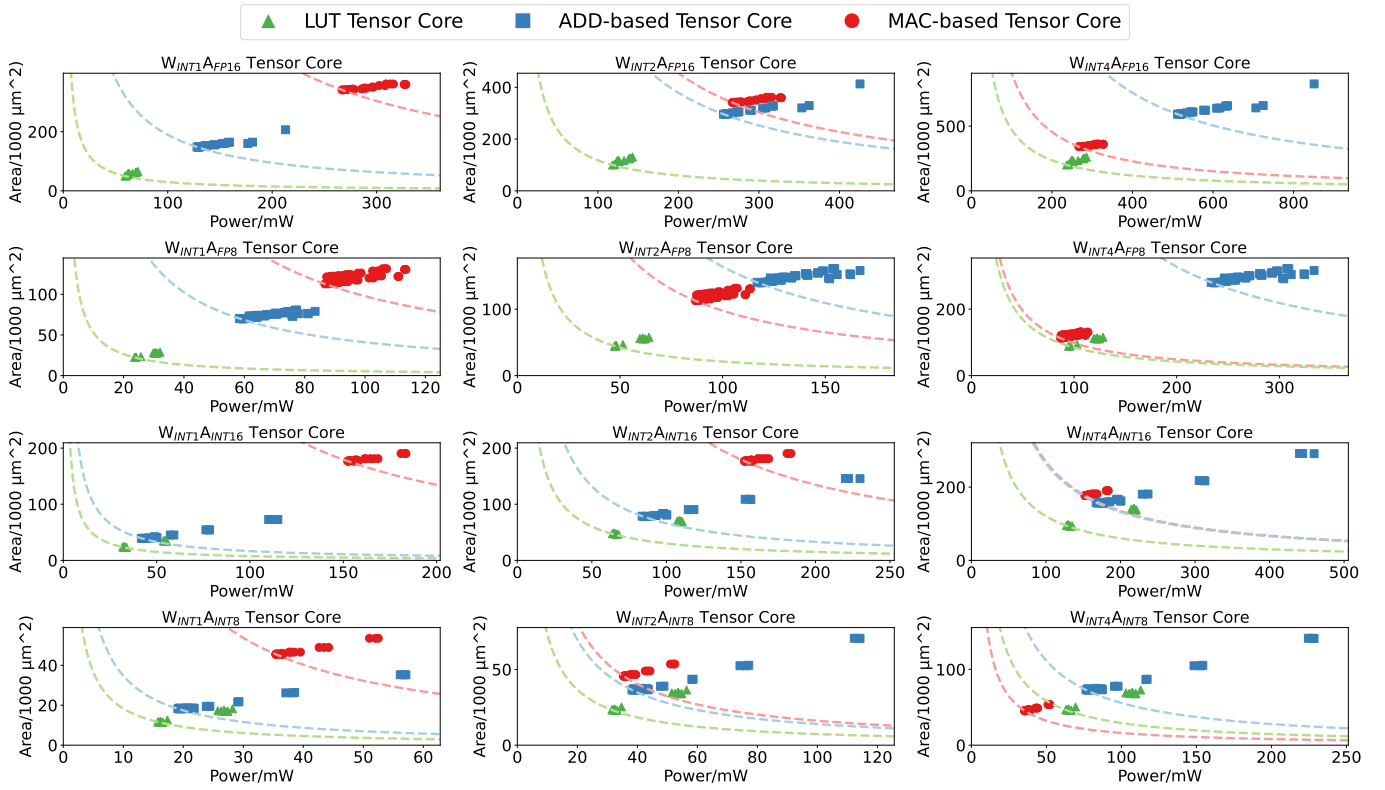


Fig. 13: PPA across LUT TENSOR CORE, ADD-based Tensor Core, and MAC-based Tensor Core implementations for mpGEMM.

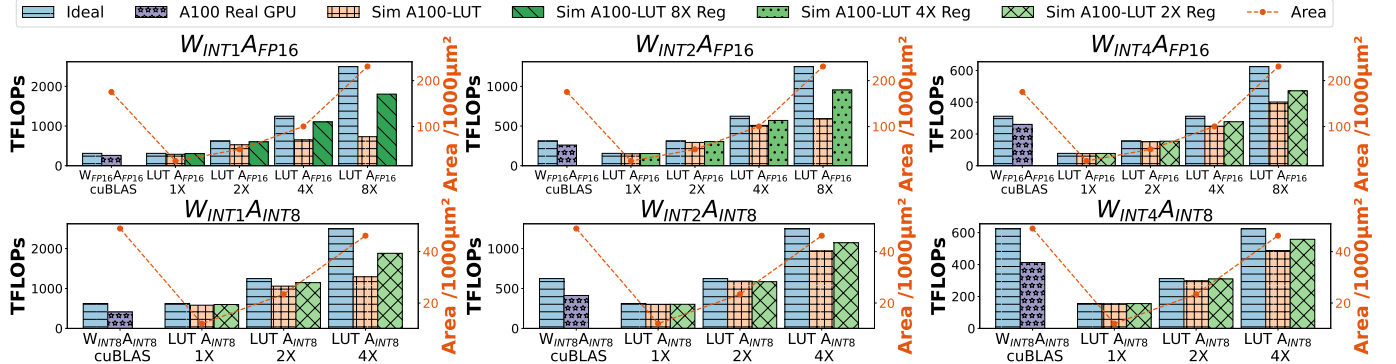


Fig. 14: Accel-Sim runtime and area across A_{FP16} and A_{INT8} LUT TENSOR CORE designs.

in mpGEMM operations under equivalent area constraints. For instance, using $W_{INT1}A_{FP16}$, the LUT TENSOR CORE approach achieves slightly higher mpGEMM performance while occupying only 14.3% the area of a MAC-based Tensor Core. With a modest 31.6% increase in area, incorporating more registers, the LUT configuration achieves a $6.9\times$ acceleration in mpGEMM operations.

D. Model End-to-End Evaluation

While Accel-Sim offers detailed architectural emulation, it suffers from a slowdown of approximately five million times, transforming a ten-second task on an A100 GPU into a

simulation period of up to 579 days, and generating trace files over 79TB in size. These limitations hinder comprehensive end-to-end assessments.

To overcome these obstacles, we have developed an end-to-end simulator designed for rapid and accurate emulation with tile-level granularity. Our insight is that the behavior of highly optimized, large GPU kernels with minimal stalling can be treated as accelerators, particularly in LLM scenarios. This viewpoint is corroborated by findings from NVIDIA in NVAS [59], which suggests viewing GPU simulation philosophically as “dynamically interacting roofline components”, rather than as a “cycle-by-cycle progression”. Accordingly,

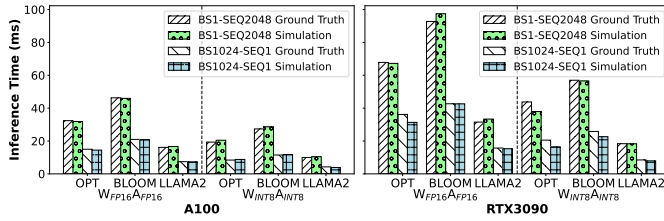


Fig. 15: Evaluation of end-to-end simulator accuracy.

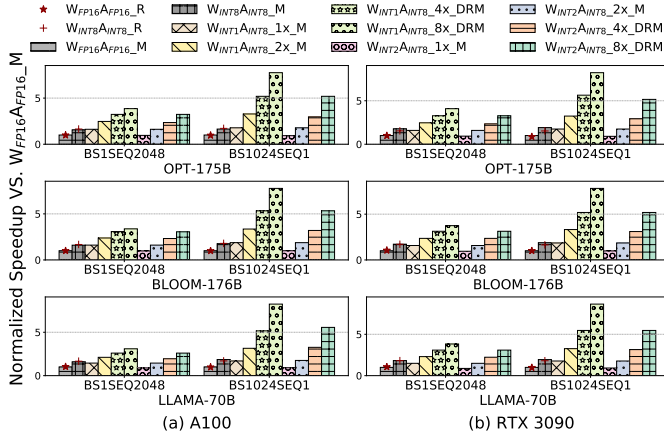


Fig. 16: End-to-end simulation results on LLMs (A100 and 3090). *R*: Real GPU, *M*: Modeling, *DR*: Double Reg

we leverage analytical methods from established accelerator modeling practices, such as Timeloop [44], Maestro [30], and Tileflow [74], to develop a tile-based GPU simulator. This tool enables detailed and accurate assessments of dataflow, memory bandwidth, computational resources, and operator fusion. We plan to open-source this simulator in future work.

1) **Simulator accuracy evaluation**: In Fig. 15, we validate our end-to-end simulator using three representative LLMs: OPT-175B [71], BLOOM-176B [32], and LLAMA2-70B [57], across various configurations on a single layer on both the A100 and RTX 3090 GPUs. Our simulator achieves a mean absolute percentage error of only 5.21% against real GPU performance, while significantly faster than Accel-Sim in simulation speed.

2) **End-to-End inference simulation results**: Following validation, Fig. 16 presents the benchmark results for the OPT, BLOOM, and LLAMA models. Our experiments reveal that, although many operators are not accelerated by Tensor Cores, the $W_{INT1}A_{INT8}$ LUT TENSOR CORE achieve theoretical peak compute performance up to $16\times$ higher than traditional $W_{FP16}A_{FP16}$ Tensor Cores, while occupying only 38% of the area. Despite the theoretical improvement, the actual end-to-end performance improvement is up to $8.2\times$. This demonstrates that, as GEMM operations dominate in the encoding phases of LLMs and in large batch decoding, accelerated GEMM can often translate into significant end-to-end speedups in many scenarios.

TABLE I: Comparison of separated table precompute and fused table precompute. With operator fusion, the table precompute overhead is negligible.

Model	Config	Welder	Welder +precompute	Welder +Fused precompute
OPT-175B	BS1SEQ2048	32.38 ms	38.77 ms	33.63 ms
OPT-175B	BS1024SEQ1	14.99 ms	17.43 ms	15.50 ms
BLOOM-176B	BS1SEQ4096	107.11 ms	129.85 ms	108.38 ms
BLOOM-176B	BS1024SEQ1	20.99 ms	26.05 ms	21.31 ms
LLAMA2-70B	BS1SEQ4096	34.68 ms	37.60 ms	35.65 ms
LLAMA2-70B	BS1024SEQ1	11.45 ms	15.21 ms	11.75 ms

TABLE II: Table quantization analysis on LLAMA2-7B.

# Bits	WikiText2 PPL ↓	MMLU 5s ↑	Zero-shot Accuracy ↑					
			HS	BQ	OQ	PQ	WGe Avg.	
$W_{INT2}A_{FP16}$	7.68	30.45	49.19	70.24	25.80	73.78	63.06	56.41
$W_{INT2}A_{LUT_INT8}$	7.69	30.61	49.17	70.00	26.20	73.67	63.54	56.52

E. Software Optimization Analysis

1) **Table precompute fusion analysis**: Table I demonstrates the impact of incorporating precomputation with the DNN compiler Welder [54], designed to enhance inference performance by optimizing operator fusion. This evaluation was conducted on a single layer of the OPT-175B, BLOOM-176B, and LLAMA2-70B models in both batch prefill and decoding configurations. Initially, precomputation on CUDA Cores led to average overheads of 16.47% and 24.41%. However, by delegating precomputation as an independent operator within Welder’s search space, overheads reduced dramatically to 2.62% and 2.52%, thus becoming negligible in the overall execution time.

2) **Table quantization analysis**: To evaluate the impact of table quantization as introduced in Section III-A3, we conduct a comparative experiments on a LLAMA2-7B model with 2-bit quantized weights. The 2-bit model is derived from BitDistiller [14], which is an open-source state-of-the-art model. The original configuration comprised INT2 weights and FP16 activations. Building upon the open-sourced code of BitDistiller, we further implemented INT8 table quantization with LUT-based mpGEMM. The evaluation metrics, align with BitDistiller, included perplexity on the WikiText-2 dataset [41], 5-shot accuracy on MMLU [19], and zero-shot accuracy across several tasks [5], [9], [43], [51], [70]. The results of this empirical study are summarized in Table II. Notably, the INT8 table quantization does not compromise model accuracy, with a negligible degradation in perplexity and a very slight increase in task accuracy, which may be attributed to the regularizing effect of quantization.

F. Comparisons

1) **Overall comparison**: To provide a comprehensive assessment of the LLM model’s accuracy, inference throughput, and PE area under mpGEMM, Table III presents an extensive evaluation. With nearly identical accuracy, the A100 equipped with LUT + BitNet achieves up to a $6.93\times$ acceleration in inference speed while utilizing only 38.3% of the original Tensor Core’s area. This results in an increase of up to $20.9\times$ in compute density and an $11.2\times$ improvement in

TABLE III: Overall comparison of full-precision LLM on A100 and low-bit LLM on LUT TENSOR CORE-equipped A100.

HW. Config.	Model	Model Avg. Acc.	BS1 SEQ2048 Latency	BS1024 SEQ1 Latency	Peak Perf.	TC. Area Per SM	TC. Compute Density	TC. Energy Efficiency
A100	LLAMA 3B ($W_{FP16}A_{FP16}$)	49.7%	119.70ms	51.75ms	312 TFLOPs	0.975mm ²	2.96TFLOPs/mm ²	2.98 TFLOPs/W
A100-LUT-4X*	BitNet b1.58 3B ($W_{INT2}A_{INT8}$)	49.4%	42.49ms	11.41ms	1248 TOPs	0.187mm ²	61.84TOPs/mm ²	33.32 TOPs/W
A100-LUT-8X*	BitNet b1.58 3B ($W_{INT2}A_{INT8}$)	49.4%	38.02ms	7.47ms	2496 TOPs	0.373mm ²	61.95TOPs/mm ²	33.65 TOPs/W

Note: Given the absence of public data on the A100 Tensor Core area, and the fact that the A100 utilizes a 7nm process while our study is based on a 28nm process, the above data represent a fair comparison. These data have been optimized to the best of our ability, based on the 28nm process, targeting 1.41GHz to align with the A100’s frequency. A100-LUT* represents LUT TENSOR CORE-equipped A100 DRM (Double Register Modeling). TC. represents Tensor Core.

TABLE IV: Comparison of related works.

	UNPU [34]	Ant [18]	Mokey [69]	FIGNA [24]	LUT TENSOR CORE
Act. Format	INT16	flint4	FP16/32, INT4	FP16/32, BF16	FP/INT8, FP/INT16
Wgt. Format	INT1~INT16	flint4	INT3/4	INT4/8	INT1~INT4
Compute Engine	LUT	flint-flint MAC	Multi Counter	Pre-aligned INT MAC	LUT
Process	65nm	28nm	65nm	28nm	28nm
PE Energy Eff.	27TOPs/W @0.9V ($W_{INT1}A_{INT16}$)	N/A	N/A	2.19X FP16-FP16 ($W_{INT4}A_{FP16}$)	63.78TOPs/W @0.9V DC ($W_{INT1}A_{INT8}$)
Compiler Stack	✗	✗	✗	✗	✓
Evaluated Models	VGG-16, AlexNet	ResNet-18, BERT	BERT, Ro/DeBERTa	BERT, BLOOM, OPT	LLAMA, BitNet, BLOOM, OPT

energy efficiency, thanks to the quantized LUT table and highly optimized LUT circuit through software-hardware co-design. These improvements maintain comparable LLM accuracy while significantly enhancing performance and efficiency.

2) **Compared to prior works:** In comparison to prior works [18], [24], [34], [69] in hardware acceleration based on quantization, diverse computational engines, such as LUTs and MACs, have been employed. Each methodology entails distinct choices regarding weight and activation quantization formats, reflecting varied implementation strategies. While direct performance metrics like energy efficiency (TOPs/W) and area efficiency (TOPs/mm²) are not explicitly provided in the literature due to differences in benchmarking setups and target backends, the orthogonal nature of these methodologies presents intriguing opportunities.

V. DISCUSSION AND LIMITATION

Low-Bit Training and Finetuning. LUT TENSOR CORE primarily focuses on the inference acceleration for low-bit LLMs. Recent trends show an increasing interest in low-bit training and fine-tuning for LLMs [11], [63]. While LUT TENSOR CORE’s approach for mpGEMM is applicable during the forward pass of low-bit training, the complexity and stability of the training process still demand more high precision computation in the backward pass. This involves tensors and calculations such as gradients and optimizer states, which are not yet fully compatible with low-bit formats at present. Further, the efficiency of training is impacted by a broad spectrum of factors such as memory efficiency and communication efficiency, beyond the just GEMM performance. Consequently, optimizing the low-bit training process requires a comprehensive strategy, possibly entailing new training algorithms

that can embrace lower precision and hardware innovations to support the intricate requirements of training workflows. We identify these as potential future directions for extending LUT TENSOR CORE to the training domain.

Long Context Attention and KV Cache Quantization. Addressing long contexts is an important frontier for LLM capabilities [13], [48]. In long context scenarios, the attention mechanism often becomes the computational bottleneck. Current research and practice indicate that during the pre-filling stage, quantizing attention computation to FP8 does not significantly compromise model accuracy [52]. However, the implications of reducing precision to ultra-low bit levels for model accuracy remain unexplored. During the decoding phase, several studies have shown that quantizing the KV cache to 4-bit or even 2-bit has a negligible impact on model performance [21], [37]. Given that the Q matrix remains in high precision, the computation aligns with mpGEMM. Exploring LUT TENSOR CORE’s potential in long context scenarios stands out as a promising future direction.

VI. RELATED WORK

Low-Bit DNN Accelerators. As deep learning models, particularly LLMs, grow in size, there is an increasing need for low-bit quantization techniques to reduce model size and computational requirements. This has naturally led to the development of hardware accelerators to meet the requirements of lower bit-width data types for efficient quantized model inference. NVIDIA’s GPU architecture advancements reflect the shift towards supporting lower precision operations. Starting with the Fermi architecture’s support for FP32 and FP64, subsequent architectures have progressively included

lower bit-width formats such as FP16 in Pascal, INT4 and INT8 in Turing, and BF16 in Ampere. In the era of LLMs, Hopper has introduced FP8 [42] and Blackwell has advanced to FP4 [49]. Beyond GPUs, recent studies propose customized accelerators that specifically target low-bit quantized DNNs [18], [31], [38], [50], [68], [69]. These advances demonstrate significant progress, they predominantly focus on GEMM operations where both inputs (weights and activations) share the same datatype and bit-width. FIGNA [24] customizes an $W_{INT4}A_{FP16}$ arithmetic unit for enhanced low-bit LLM inference. However, supporting a wide range of precision combinations in hardware necessitates a more complex design and increased chip area. LUT TENSOR CORE improves the efficiency of mpGEMM with LUT-based computing paradigm, and offers the flexibility to support diverse precision combinations without the need for complex hardware redesigns.

Sparse DNN Accelerators. In conjunction with low-bit quantization, sparsity is another popular strategy to reduce model size and accelerate DNN inference. Sparsity leverages the inherent zero-valued elements within DNN weight matrices or activations, omitting them from computation and storage to improve efficiency. With the advent of the NVIDIA A100 GPU, Sparse Tensor Cores have been introduced, offering native support for sparsity by facilitating 2:4 structured sparsity [8]. Beyond commercial GPUs, there has been a surge in customized sparse DNN accelerators. These designs are tailored to exploit sparsity to varying degrees, often employing techniques such as pruning, zero-skipping, and sparse matrix formats to optimize both storage and computation [16], [22], [23], [53], [62], [65], [76]. Sparsity is also prevalent in low-bit LLMs. When combined with quantization, sparsity has the potential to yield even more substantial efficiency gains. However, effectively integrating both quantization and sparsity presents a significant challenges in maintaining model accuracy and customizing microarchitectures. The integration of sparsity into LUT TENSOR CORE represents a promising research direction, which we leave as future exploration.

VII. CONCLUSION

This paper presents the LUT TENSOR CORE, a software-hardware co-design with LUT-based computing paradigm to enable efficient mixed-precision GEMM operations for low-bit LLM acceleration. LUT TENSOR CORE can significantly boost computational performance, provide extensive flexibility for various precision combinations, and smoothly integrate with existing accelerator architecture and software ecosystems.

REFERENCES

- [1] "llama.cpp," <https://github.com/ggerganov/llama.cpp>.
- [2] "NVIDIA CUTLASS," <https://github.com/NVIDIA/cutlass>.
- [3] "NVIDIA TensorRT-LLM," <https://github.com/NVIDIA/TensorRT-LLM>.
- [4] J. Achiam, S. Adler, S. Agarwal, L. Ahmad, I. Akkaya, F. L. Aleman, D. Almeida, J. Altschmidt, S. Altman, S. Anadkat *et al.*, "Gpt-4 technical report," *arXiv preprint arXiv:2303.08774*, 2023.
- [5] Y. Bisk, R. Zellers, R. L. Bras, J. Gao, and Y. Choi, "Piqa: Reasoning about physical commonsense in natural language," 2019.
- [6] T. Brown, B. Mann, N. Ryder, M. Subbiah, J. D. Kaplan, P. Dhariwal, A. Neelakantan, P. Shyam, G. Sastry, A. Askell *et al.*, "Language models are few-shot learners," *Advances in neural information processing systems*, vol. 33, pp. 1877–1901, 2020.
- [7] T. Chen, T. Moreau, Z. Jiang, H. Shen, E. Q. Yan, L. Wang, Y. Hu, L. Ceze, C. Guestrin, and A. Krishnamurthy, "Tvm: end-to-end optimization stack for deep learning," *arXiv preprint arXiv:1802.04799*, vol. 11, no. 20, 2018.
- [8] J. Choquette, W. Gandhi, O. Giroux, N. Stam, and R. Krashinsky, "Nvidia a100 tensor core gpu: Performance and innovation," *IEEE Micro*, vol. 41, no. 2, pp. 29–35, 2021.
- [9] C. Clark, K. Lee, M.-W. Chang, T. Kwiatkowski, M. Collins, and K. Toutanova, "Boolq: Exploring the surprising difficulty of natural yes/no questions," 2019.
- [10] T. Dettmers, M. Lewis, Y. Belkada, and L. Zettlemoyer, "Gpt3. int8 (0): 8-bit matrix multiplication for transformers at scale," *Advances in Neural Information Processing Systems*, vol. 35, pp. 30318–30332, 2022.
- [11] T. Dettmers, A. Pagnoni, A. Holtzman, and L. Zettlemoyer, "Qlora: Efficient finetuning of quantized llms," *Advances in Neural Information Processing Systems*, vol. 36, 2024.
- [12] T. Dettmers and L. Zettlemoyer, "The case for 4-bit precision: k-bit inference scaling laws," in *International Conference on Machine Learning*. PMLR, 2023, pp. 7750–7774.
- [13] Y. Ding, L. L. Zhang, C. Zhang, Y. Xu, N. Shang, J. Xu, F. Yang, and M. Yang, "Longrope: Extending llm context window beyond 2 million tokens," *arXiv preprint arXiv:2402.13753*, 2024.
- [14] D. Du, Y. Zhang, S. Cao, J. Guo, T. Cao, X. Chu, and N. Xu, "Bit-distiller: Unleashing the potential of sub-4-bit llms via self-distillation," *arXiv preprint arXiv:2402.10631*, 2024.
- [15] E. Frantar, S. Ashkboos, T. Hoefler, and D. Alistarh, "Gptq: Accurate post-training quantization for generative pre-trained transformers," *arXiv preprint arXiv:2210.17323*, 2022.
- [16] A. Gondimalla, M. Thottethodi, and T. Vijaykumar, "Eureka: Efficient tensor cores for one-sided unstructured sparsity in dnn inference," in *Proceedings of the 56th Annual IEEE/ACM International Symposium on Microarchitecture*, 2023, pp. 324–337.
- [17] C. Guo, J. Tang, W. Hu, J. Leng, C. Zhang, F. Yang, Y. Liu, M. Guo, and Y. Zhu, "Olive: Accelerating large language models via hardware-friendly outlier-victim pair quantization," in *Proceedings of the 50th Annual International Symposium on Computer Architecture*, 2023, pp. 1–15.
- [18] C. Guo, C. Zhang, J. Leng, Z. Liu, F. Yang, Y. Liu, M. Guo, and Y. Zhu, "Ant: Exploiting adaptive numerical data type for low-bit deep neural network quantization," in *2022 55th IEEE/ACM International Symposium on Microarchitecture (MICRO)*. IEEE, 2022, pp. 1414–1433.
- [19] D. Hendrycks, C. Burns, S. Basart, A. Zou, M. Mazeika, D. Song, and J. Steinhardt, "Measuring massive multitask language understanding," 2021.
- [20] J. Hoffmann, S. Borgeaud, A. Mensch, E. Buchatskaya, T. Cai, E. Rutherford, D. d. L. Casas, L. A. Hendricks, J. Welbl, A. Clark *et al.*, "Training compute-optimal large language models," *arXiv preprint arXiv:2203.15556*, 2022.
- [21] C. Hooper, S. Kim, H. Mohammadzadeh, M. W. Mahoney, Y. S. Shao, K. Keutzer, and A. Gholami, "Kvquant: Towards 10 million context length llm inference with kv cache quantization," *arXiv preprint arXiv:2401.18079*, 2024.
- [22] G. Huang, Z. Wang, P.-A. Tsai, C. Zhang, Y. Ding, and Y. Xie, "Rm-stc: Row-merge dataflow inspired gpu sparse tensor core for energy-efficient sparse acceleration," in *Proceedings of the 56th Annual IEEE/ACM International Symposium on Microarchitecture*, 2023, pp. 338–352.
- [23] D. Im and H.-J. Yoo, "Lutein: Dense-sparse bit-slice architecture with radix-4 lut-based slice-tensor processing units," in *2024 IEEE International Symposium on High-Performance Computer Architecture (HPCA)*. IEEE, 2024, pp. 747–759.
- [24] J. Jang, Y. Kim, J. Lee, and J.-J. Kim, "Figma: Integer unit-based accelerator design for fp-int gemm preserving numerical accuracy," in *2024 IEEE International Symposium on High-Performance Computer Architecture (HPCA)*. IEEE, 2024, pp. 760–773.
- [25] Y. Jeon, B. Park, S. J. Kwon, B. Kim, J. Yun, and D. Lee, "Biggemm: matrix multiplication with lookup table for binary-coding-based quantized dnn," in *SC20: International Conference for High Performance Computing, Networking, Storage and Analysis*. IEEE, 2020, pp. 1–14.

- [26] P. Judd, J. Albericio, T. Hetherington, T. M. Aamodt, and A. Moshovos, "Stripes: Bit-serial deep neural network computing," in *2016 49th Annual IEEE/ACM International Symposium on Microarchitecture (MICRO)*. IEEE, 2016, pp. 1–12.
- [27] J. Kaplan, S. McCandlish, T. Henighan, T. B. Brown, B. Chess, R. Child, S. Gray, A. Radford, J. Wu, and D. Amodei, "Scaling laws for neural language models," *arXiv preprint arXiv:2001.08361*, 2020.
- [28] M. Khairy, Z. Shen, T. M. Aamodt, and T. G. Rogers, "Accel-sim: An extensible simulation framework for validated gpu modeling," in *2020 ACM/IEEE 47th Annual International Symposium on Computer Architecture (ISCA)*. IEEE, 2020, pp. 473–486.
- [29] S. Kim, C. Hooper, A. Gholami, Z. Dong, X. Li, S. Shen, M. W. Mahoney, and K. Keutzer, "Squeezellm: Dense-and-sparse quantization," *arXiv preprint arXiv:2306.07629*, 2023.
- [30] H. Kwon, P. Chatarasi, V. Sarkar, T. Krishna, M. Pellauer, and A. Parashar, "Maestro: A data-centric approach to understand reuse, performance, and hardware cost of dnn mappings," *IEEE micro*, vol. 40, no. 3, pp. 20–29, 2020.
- [31] A. D. Lascorz, M. Mahmoud, A. H. Zadeh, M. Nikolic, K. Ibrahim, C. Giannoula, A. Abdelhadi, and A. Moshovos, "Atalanta: A bit is worth a "thousand" tensor values," in *Proceedings of the 29th ACM International Conference on Architectural Support for Programming Languages and Operating Systems, Volume 2*, 2024, pp. 85–102.
- [32] T. Le Scao, A. Fan, C. Akiki, E. Pavlick, S. Ilić, D. Hesslow, R. Castagné, A. S. Luccioni, F. Yvon, M. Gallé *et al.*, "Bloom: A 176b-parameter open-access multilingual language model," 2023.
- [33] C. Lee, J. Jin, T. Kim, H. Kim, and E. Park, "Owq: Lessons learned from activation outliers for weight quantization in large language models," *arXiv preprint arXiv:2306.02272*, 2023.
- [34] J. Lee, C. Kim, S. Kang, D. Shin, S. Kim, and H.-J. Yoo, "Unpu: An energy-efficient deep neural network accelerator with fully variable weight bit precision," *IEEE Journal of Solid-State Circuits*, vol. 54, no. 1, pp. 173–185, 2019.
- [35] J. Lin, J. Tang, H. Tang, S. Yang, X. Dang, and S. Han, "Awq: Activation-aware weight quantization for llm compression and acceleration," *arXiv preprint arXiv:2306.00978*, 2023.
- [36] J. Liu, R. Gong, X. Wei, Z. Dong, J. Cai, and B. Zhuang, "Qllm: Accurate and efficient low-bitwidth quantization for large language models," 2024.
- [37] Z. Liu, J. Yuan, H. Jin, S. Zhong, Z. Xu, V. Braverman, B. Chen, and X. Hu, "Kivi: A tuning-free asymmetric 2bit quantization for kv cache," *arXiv preprint arXiv:2402.02750*, 2024.
- [38] Y.-C. Lo and R.-S. Liu, "Bucket getter: A bucket-based processing engine for low-bit block floating point (bfp) dnns," in *Proceedings of the 56th Annual IEEE/ACM International Symposium on Microarchitecture*, ser. MICRO '23. New York, NY, USA: Association for Computing Machinery, 2023, p. 1002–1015. [Online]. Available: <https://doi.org/10.1145/3613424.3614249>
- [39] S. Ma, H. Wang, L. Ma, L. Wang, W. Wang, S. Huang, L. Dong, R. Wang, J. Xue, and F. Wei, "The era of 1-bit llms: All large language models are in 1.58 bits," *arXiv preprint arXiv:2402.17764*, 2024.
- [40] S. Maleki, "Look-up mai gemm: Increasing ai gemms performance by nearly 2.5 x via msgemm," *arXiv preprint arXiv:2310.06178*, 2023.
- [41] S. Merity, C. Xiong, J. Bradbury, and R. Socher, "Pointer sentinel mixture models," 2016.
- [42] P. Micikevicius, D. Stosic, N. Burgess, M. Cornea, P. Dubey, R. Grisenthwaite, S. Ha, A. Heinecke, P. Judd, J. Kamalu *et al.*, "Fp8 formats for deep learning," *arXiv preprint arXiv:2209.05433*, 2022.
- [43] T. Mihaylov, P. Clark, T. Khot, and A. Sabharwal, "Can a suit of armor conduct electricity? a new dataset for open book question answering," 2018.
- [44] A. Parashar, P. Raina, Y. S. Shao, Y.-H. Chen, V. A. Ying, A. Mukkara, R. Venkatesan, B. Khailany, S. W. Keckler, and J. Emer, "Timeloop: A systematic approach to dnn accelerator evaluation," in *2019 IEEE international symposium on performance analysis of systems and software (ISPASS)*. IEEE, 2019, pp. 304–315.
- [45] G. Park, B. Park, M. Kim, S. Lee, J. Kim, B. Kwon, S. J. Kwon, B. Kim, Y. Lee, and D. Lee, "Lut-gemm: Quantized matrix multiplication based on luts for efficient inference in large-scale generative language models," *arXiv preprint arXiv:2206.09557*, 2023.
- [46] P. Patel, E. Choukse, C. Zhang, A. Shah, Í. Goiri, S. Maleki, and R. Bianchini, "Splitwise: Efficient generative llm inference using phase splitting," *Power*, vol. 400, no. 700W, pp. 1–75, 2023.
- [47] D. Patterson, J. Gonzalez, U. Hölzle, Q. Le, C. Liang, L.-M. Munguia, D. Rothchild, D. R. So, M. Texier, and J. Dean, "The carbon footprint of machine learning training will plateau, then shrink," *Computer*, vol. 55, no. 7, pp. 18–28, 2022.
- [48] B. Peng, J. Quesnelle, H. Fan, and E. Shippole, "Yarn: Efficient context window extension of large language models," *arXiv preprint arXiv:2309.00071*, 2023.
- [49] B. D. Rouhani, R. Zhao, A. More, M. Hall, A. Khodamoradi, S. Deng, D. Choudhary, M. Cornea, E. Dellinger, K. Denolf *et al.*, "Microscaling data formats for deep learning," *arXiv preprint arXiv:2310.10537*, 2023.
- [50] S. Ryu, H. Kim, W. Yi, E. Kim, Y. Kim, T. Kim, and J.-J. Kim, "Bitblade: Energy-efficient variable bit-precision hardware accelerator for quantized neural networks," *IEEE Journal of Solid-State Circuits*, vol. 57, no. 6, pp. 1924–1935, 2022.
- [51] K. Sakaguchi, R. L. Bras, C. Bhagavatula, and Y. Choi, "Winogrande: An adversarial winograd schema challenge at scale," 2019.
- [52] J. Shah, G. Bikshandi, Y. Zhang, V. Thakkar, P. Ramani, and T. Dao, "Flashattention-3: Fast and accurate attention with asynchrony and low-precision," *arXiv preprint arXiv:2407.08608*, 2024.
- [53] M. Shi, V. Jain, A. Joseph, M. Meijer, and M. Verhelst, "Bitwave: Exploiting column-based bit-level sparsity for deep learning acceleration," in *2024 IEEE International Symposium on High-Performance Computer Architecture (HPCA)*. IEEE, 2024, pp. 732–746.
- [54] Y. Shi, Z. Yang, J. Xue, L. Ma, Y. Xia, Z. Miao, Y. Guo, F. Yang, and L. Zhou, "Welder: Scheduling deep learning memory access via tile-graph," in *17th USENIX Symposium on Operating Systems Design and Implementation (OSDI 23)*, 2023, pp. 701–718.
- [55] Synopsys Inc., *Design Compiler User Guide*, 2018.
- [56] G. Team, R. Anil, S. Borgeaud, Y. Wu, J.-B. Alayrac, J. Yu, R. Soricut, J. Schalkwyk, A. M. Dai, A. Hauth *et al.*, "Gemini: a family of highly capable multimodal models," *arXiv preprint arXiv:2312.11805*, 2023.
- [57] H. Touvron, L. Martin, K. Stone, P. Albert, A. Almahairi, Y. Babaei, N. Bashlykov, S. Batra, P. Bhargava, S. Bhosale *et al.*, "Llama 2: Open foundation and fine-tuned chat models," *arXiv preprint arXiv:2307.09288*, 2023.
- [58] A. Vaswani, N. Shazeer, N. Parmar, J. Uszkoreit, L. Jones, A. N. Gomez, Ł. Kaiser, and I. Polosukhin, "Attention is all you need," *Advances in neural information processing systems*, vol. 30, 2017.
- [59] O. Villa, D. Lustig, Z. Yan, E. Bolotin, Y. Fu, N. Chatterjee, N. Jiang, and D. Nellans, "Need for speed: Experiences building a trustworthy system-level gpu simulator," in *2021 IEEE International Symposium on High-Performance Computer Architecture (HPCA)*. IEEE, 2021, pp. 868–880.
- [60] H. Wang, S. Ma, L. Dong, S. Huang, H. Wang, L. Ma, F. Yang, R. Wang, Y. Wu, and F. Wei, "Bitnet: Scaling 1-bit transformers for large language models," *arXiv preprint arXiv:2310.11453*, 2023.
- [61] L. Wang, L. Ma, S. Cao, Q. Zhang, J. Xue, Y. Shi, N. Zheng, Z. Miao, F. Yang, T. Cao *et al.*, "Ladder: Enabling efficient {Low-Precision} deep learning computing through hardware-aware tensor transformation," in *18th USENIX Symposium on Operating Systems Design and Implementation (OSDI 24)*, 2024, pp. 307–323.
- [62] Y. Wang, C. Zhang, Z. Xie, C. Guo, Y. Liu, and J. Leng, "Dual-side sparse tensor core," in *2021 ACM/IEEE 48th Annual International Symposium on Computer Architecture (ISCA)*. IEEE, 2021, pp. 1083–1095.
- [63] H. Xi, C. Li, J. Chen, and J. Zhu, "Training transformers with 4-bit integers," *Advances in Neural Information Processing Systems*, vol. 36, pp. 49 146–49 168, 2023.
- [64] G. Xiao, J. Lin, M. Seznec, H. Wu, J. Demouth, and S. Han, "Smoothquant: Accurate and efficient post-training quantization for large language models," in *International Conference on Machine Learning*. PMLR, 2023, pp. 38 087–38 099.
- [65] J. Yang, Z. Zhang, Z. Liu, J. Zhou, L. Liu, S. Wei, and S. Yin, "Fusekna: Fused kernel convolution based accelerator for deep neural networks," in *2021 IEEE International Symposium on High-Performance Computer Architecture (HPCA)*. IEEE, 2021, pp. 894–907.
- [66] Z. Yao, R. Yazdani Aminabadi, M. Zhang, X. Wu, C. Li, and Y. He, "Zeroquant: Efficient and affordable post-training quantization for large-scale transformers," *Advances in Neural Information Processing Systems*, vol. 35, pp. 27 168–27 183, 2022.
- [67] A. Young, B. Chen, C. Li, C. Huang, G. Zhang, G. Zhang, H. Li, J. Zhu, J. Chen, J. Chang *et al.*, "Yi: Open foundation models by 01. ai," *arXiv preprint arXiv:2403.04652*, 2024.

- [68] A. H. Zadeh, I. Edo, O. M. Awad, and A. Moshovos, “Gobo: Quantizing attention-based nlp models for low latency and energy efficient inference,” in *2020 53rd Annual IEEE/ACM International Symposium on Microarchitecture (MICRO)*. IEEE, Oct. 2020. [Online]. Available: <http://dx.doi.org/10.1109/MICRO50266.2020.00071>
- [69] A. H. Zadeh, M. Mahmoud, A. Abdelhadi, and A. Moshovos, “Mokey: enabling narrow fixed-point inference for out-of-the-box floating-point transformer models,” in *Proceedings of the 49th Annual International Symposium on Computer Architecture*, ser. ISCA '22. ACM, Jun. 2022. [Online]. Available: <http://dx.doi.org/10.1145/3470496.3527438>
- [70] R. Zellers, A. Holtzman, Y. Bisk, A. Farhadi, and Y. Choi, “Hellaswag: Can a machine really finish your sentence?” 2019.
- [71] S. Zhang, S. Roller, N. Goyal, M. Artetxe, M. Chen, S. Chen, C. Dewan, M. Diab, X. Li, X. V. Lin *et al.*, “Opt: Open pre-trained transformer language models,” *arXiv preprint arXiv:2205.01068*, 2022.
- [72] Y. Zhang, L. Zhao, S. Cao, W. Wang, T. Cao, F. Yang, M. Yang, S. Zhang, and N. Xu, “Integer or floating point? new outlooks for low-bit quantization on large language models,” *arXiv preprint arXiv:2305.12356*, 2023.
- [73] L. Zheng, C. Jia, M. Sun, Z. Wu, C. H. Yu, A. Haj-Ali, Y. Wang, J. Yang, D. Zhuo, K. Sen, J. E. Gonzalez, and I. Stoica, “Anso: Generating High-Performance tensor programs for deep learning,” in *14th USENIX Symposium on Operating Systems Design and Implementation (OSDI 20)*. USENIX Association, Nov. 2020, pp. 863–879. [Online]. Available: <https://www.usenix.org/conference/osdi20/presentation/zheng>
- [74] S. Zheng, S. Chen, S. Gao, L. Jia, G. Sun, R. Wang, and Y. Liang, “Tileflow: A framework for modeling fusion dataflow via tree-based analysis,” in *Proceedings of the 56th Annual IEEE/ACM International Symposium on Microarchitecture*, 2023, pp. 1271–1288.
- [75] H. Zhu, R. Wu, Y. Diao, S. Ke, H. Li, C. Zhang, J. Xue, L. Ma, Y. Xia, W. Cui *et al.*, “{ROLLER}: Fast and efficient tensor compilation for deep learning,” in *16th USENIX Symposium on Operating Systems Design and Implementation (OSDI 22)*, 2022, pp. 233–248.
- [76] M. Zhu, T. Zhang, Z. Gu, and Y. Xie, “Sparse tensor core: Algorithm and hardware co-design for vector-wise sparse neural networks on modern gpus,” in *Proceedings of the 52nd Annual IEEE/ACM International Symposium on Microarchitecture*, 2019, pp. 359–371.